Long-Range and Local Circuits for Top-Down Modulation of Visual Cortical Processing

Siyu Zhang[1], **Min Xu**[1], **Tsukasa Kamigaki**[1], **Johnny Phong Hoang Do**[1], **Wei-Cheng Chang**[1], **Sean Jenvay**[1], **Kazunari Miyamichi**[2,†], **Liqun Luo**[2], and **Yang Dan**[1,*]

[1]Division of Neurobiology, Department of Molecular and Cell Biology, Helen Wills Neuroscience Institute, Howard Hughes Medical Institute, University of California, Berkeley, California 94720, USA

[2]Department of Biology, Howard Hughes Medical Institute, Stanford University, Stanford, California 94305, USA

Abstract

Top-down modulation of sensory processing allows the animal to select inputs most relevant to current tasks. We found that the cingulate (Cg) region of mouse frontal cortex powerfully influences sensory processing in primary visual cortex (V1) through long-range projections that activate local GABAergic circuits. Optogenetic activation of Cg neurons enhanced V1 neuron responses and improved visual discrimination. Focal activation of Cg axons in V1 caused a response increase at the activation site but decrease at nearby locations (center-surround modulation). While somatostatin-positive GABAergic interneurons contributed preferentially to surround suppression, vasoactive intestinal peptide-positive interneurons were crucial for center facilitation. Long-range cortico-cortical projections thus act through local microcircuits to exert spatially specific top-down modulation of sensory processing.

Sensory processing is strongly modulated by the animal's behavioral state. A well-known example is top-down attention, a powerful mechanism for selective processing of behaviorally relevant information and filtering out irrelevant stimuli. In visual cortical areas, many neurons exhibit enhanced responses to attended stimuli (1–4). Several frontal and parietal cortical regions have been implicated as the sources of top-down modulation signals (1, 2, 5, 6), especially the dorsolateral prefrontal cortex and frontal eye field (FEF) (7–13). Electrical stimulation of the FEF enhanced V4 neuron responses at the retinotopically corresponding location and suppressed responses at other locations (11), resembling the center-surround profile of attentional modulation (1, 3, 14, 15). Beyond identifying the signal sources, however, the synaptic circuits mediating top-down modulation are largely unknown. In addition to cortico-cortical projections, FEF also projects to the thalamus and other subcortical circuits that modulate cortical processing (16–20). The role of each pathway has not been clearly delineated. Furthermore, as long-range cortico-cortical

[*]To whom correspondence should be addressed. ydan@berkeley.edu.
[†]Present address: the University of Tokyo, Japan

projections are primarily glutamatergic, whether and how they provide center-surround modulation is unknown.

To examine the circuit mechanism of top-down modulation in mouse brain, we first identified neurons in the frontal cortex that directly project to visual cortex by injecting fluorescent latex microspheres (Retrobeads) into V1. We found numerous retrogradely labeled neurons in the Cg area (Fig. 1, A to C, fig. S1, A and B). To visualize the axonal projections from Cg excitatory neurons, we injected adeno-associated virus [AAV-CaMKIIα-hChR2(H134R)-EYFP] into Cg. We found EYFP-labeled axons in both V1 and surrounding visual areas, with the axons in V1 preferentially distributed in layers 1 and 6 (Fig. 1E, fig. S1C). Cg neurons also project to the superior colliculus (Fig. 1, D and E) (21).

To test the functional influence of Cg neuron activity on visual processing, we applied laser stimulation to Cg of the mouse injected with AAV-CaMKIIα-hChR2(H134R)-EYFP (Fig. 2A), which evoked reliable neuronal spiking (Fig. 2B). Cell-attached recordings in V1 of anesthetized mice measured neuronal responses to drifting grating stimuli in both control (laser-off) and Cg activation (laser-on) trials. Cg activation strongly increased V1 neuron firing rate at the preferred orientation but not at non-preferred orientation (Fig. 2C). This resulted in an approximately multiplicative scaling of the tuning curve (Fig. 2, C and D), similar to the effects of top-down attention (22) and FEF stimulation (11). Cg activation also increased the slope of V1 neuron response as a function of stimulus contrast (contrast-response function) (fig. S2B). In control mice not injected with AAV, laser stimulation had no effect (fig. S2, C and D), and the laser-induced response increase was significantly higher in the ChR2 than control mice ($P = 8 \times 10^{-4}$, t-test).

To further test the functional significance of Cg activity, we applied optogenetic manipulations in awake mice. Cg activation enhanced V1 responses at a level comparable to that in anesthetized mice (Fig. 2, D and E). Conversely, inactivation of Cg excitatory neurons significantly decreased V1 responses. Stimulation of primate FEF not only enhances visual cortical responses, but also improves perceptual performance (23). We thus tested the behavioral effect of Cg activation in mice trained to perform a visual discrimination task. Cg activation significantly improved the performance (Fig. 2F, $P < 0.02$ for each of 5 mice, paired t-test). In control mice injected with AAV-CaMKIIα-mCherry, laser had no effect ($P > 0.42$), and the laser-induced improvement was significantly greater for the ChR2 than control mice ($P = 8 \times 10^{-4}$, t-test). Note that the laser stimulation used in these experiments evoked no significant eye movement, although stimulation at much higher laser power and frequencies could evoke saccade-like movement (data not shown).

In principle, Cg neuron activity can influence V1 processing through either the direct projection or indirect pathways via other brain structures. To test whether the direct projection is sufficient for the modulation, we optogenetically activated Cg axons in V1 of anesthetized mice (Fig. 3A). Laser stimulation in a small area (~200 μm in diameter) encompassing the recorded cell (Fig. 3B) increased both the tuning curve amplitude (Fig. 3, C and D, left) and contrast-response slope (fig. S3). The magnitude of increase was ~70% of that induced by Cg neuron activation (Fig. 2, D and E).

In primate both top-down attention and FEF stimulation exert center-surround modulation of visual cortical responses (1, 3, 11, 14, 15). We next systematically varied the location of laser stimulation relative to the recorded cell (Fig. 3B). Laser stimulation at 200 μm significantly decreased the tuning curve amplitude (Fig. 3, C and D, right). The spatial profile of response modulation consisted of a facilitatory center and a suppressive surround (Fig. 3E), reminiscent of the effects of top-down attention (1, 3, 14, 15) and FEF stimulation (11). Activation of Cg axons could antidromically induce spiking of the cell bodies, which may activate axon collaterals to other brain areas. We thus repeated the axon stimulation experiment after blocking spiking in Cg with 2% lidocaine. Similar center-surround modulation was still observed in V1 (fig. S4).

Because the Cg→V1 projections activated in our experiments are glutamatergic, the center-surround modulation is likely to involve V1 local circuits. We therefore made whole-cell recordings in V1 slices. Because the topical laser stimulation used *in vivo* (Fig. 3, A and B) is likely to activate Cg axons in layer 1 preferentially, in slice experiments we also stimulated layer 1 axons (fig. S5A). We found both excitatory and inhibitory postsynaptic currents (EPSCs and IPSCs) in layer 2/3 pyramidal neurons near the laser stimulation site (fig. S5B). The EPSCs showed short onset latencies (1.9 ± 0.1 ms, mean $\pm$ SEM), suggesting monosynaptic inputs from Cg axons. However, the IPSCs showed significantly longer latencies (6.2 ± 0.4 ms, $P = 5 \times 10^{-14}$, paired *t*-test) and were completely blocked by CNQX (10 μM; fig. S5C), suggesting disynaptic inhibition. We then measured the excitatory and inhibitory inputs as functions of distance between laser stimulation and the recorded cell (fig. S5, D and E). While the strength of excitatory input decreased monotonically, the inhibitory input was stronger at 200 than at 0 μm. Such a spatial profile seems well suited for generating surround suppression *in vivo* (Fig. 3E).

The Cg axon-induced disynaptic inhibition of pyramidal neurons should originate from local GABAergic neurons. Parvalbumin-positive (PV+), somatostatin-positive (SOM+), and vasoactive intestinal peptide-positive (VIP+) interneurons are three major non-overlapping populations of cortical GABAergic neurons (24, 25), and they play different roles in visual processing (26–28). To assess the role of each subtype in top-down modulation, we first measured their responses to Cg axon stimulation. Each subtype was identified by breeding loxP-flanked tdTomato reporter mice with PV-, SOM-, or VIP-Cre mice (fig. S6A). Activation of layer 1 Cg axons evoked short-latency (~3 ms) excitatory postsynaptic potentials (EPSPs) in all three interneuron subtypes, even after V1 neuron spiking was blocked with TTX (29) (fig. S6, B to G). Rabies virus-mediated monosynaptic retrograde tracing (30) confirmed that all three subtypes received direct Cg innervation (fig. S7). The Cg input was stronger in VIP+ than the other neuron types in layer 2/3 (fig. S6), similar to the motor→somatosensory cortex input (31).

We next measured the contribution of each interneuron subtype to disynaptic inhibition of pyramidal neurons using optogenetic inactivation. To express halorhodopsin (Halo) in each subtype, we crossed PV-, SOM-, or VIP-Cre mice with loxP-flanked Halo reporter mice (32). ChR2 was expressed in Cg excitatory neurons using AAV-CaMKIIα-hChR2(H134R)-EYFP. Inactivation of PV+ neurons (yellow laser, in an area >600 μm in diameter, Fig. 4A) reduced Cg axon-induced inhibitory inputs at 0, 200, and 400 μm, but the strongest

inhibition was still observed at 200 μm (Fig. 4B, left). In contrast, inactivating SOM+ neurons caused the largest reduction of inhibition at 200 μm, such that the strength of inhibition decreased monotonically with distance (middle). Inactivating VIP+ neurons caused an increase in inhibition at 0 μm and no change at other locations (right). Thus, VIP+ neurons caused spatially localized disinhibition, likely by preferentially innervating SOM+ neurons (31, 33–35).

Finally, to test the roles of these interneuron subtypes in top-down modulation of visual processing, we optogenetically inactivated them while activating Cg axons *in vivo* (Fig. 4C). PV+ neuron inactivation caused similar response increases at 0, 200, and 400 μm (Fig. 4, D and E, left). Their inactivation with yellow laser alone without Cg axon stimulation also induced a response increase (Fig. 4D, yellow circle, $P = 0.01$), suggesting that the effect was partly due to a general reduction of cortical inhibition unrelated to Cg axon stimulation. SOM+ neuron inactivation caused the largest response increase at 200 μm, converting the surround suppression into a slight facilitation (Fig. 4, D and E, middle). The increase at 200 μm was greater than the effect of yellow laser alone ($P = 0.002$), indicating that SOM+ neurons contribute strongly to Cg axon-induced surround suppression. Inactivation of VIP+ neurons, on the other hand, blocked the center facilitation (at 0 μm) without affecting surround suppression (Fig. 4, D and E, right).

We identified a region of mouse frontal cortex that can exert spatially specific top-down modulation of visual processing, a hallmark of selective attention. The spatial pattern of Cg projections (Fig. 1, fig. S1) and its powerful modulation of visual processing indicate functional similarity between mouse Cg and primate FEF (although the FEF projects primarily to higher visual areas rather than V1). In primate visual cortex, top-down attention enhances the firing rates of putative inhibitory interneurons (14, 36). In our study the three subtypes of interneurons were all innervated by Cg, but they play different roles in top-down modulation. SOM+ neurons strongly inhibit pyramidal neurons in response to Cg input 200 μm away. That they also mediate suppression by visual stimuli outside of the receptive field (26) suggests that both bottom-up visual processing and top-down attentional modulation employ a common mechanism for surround suppression (37). Disinhibition of pyramidal neurons by VIP+ neurons has also been shown in somatosensory (31), visual (33), auditory and medial prefrontal (35) cortices, mediating firing rate increases induced by motor activity or reinforcement signals. In the top-down modulation studied here, the disinhibition is highly localized at the site of Cg axon activation (Fig. 4). Based on the effect of Halo-mediated inactivation of each cell type, we constructed a simple circuit diagram (Fig. 4F). The Cg→V1 projection provides direct inputs to both GABAergic and pyramidal neurons. In response to focal Cg axon activation, SOM+ and PV+ neurons inhibit pyramidal neurons over a broad cortical area (with SOM+ neurons as a major source of inhibition at 200 μm), whereas VIP+ neurons selectively enhance the responses at 0 μm through localized inhibition of SOM+ neurons (Fig. 4F, left). In contrast, activation of the Cg region induced only facilitation and no suppression (Fig. 2). This may be because, given the orientation and small size of Cg (Fig. 1B), topical laser stimulation inevitably activates a large proportion of V1-projecting neurons, causing broad activation of VIP+ neurons that overrides SOM-mediated surround inhibition (Fig. 4F, right). On the other hand, dual retrograde tracing

suggests that individual Cg neurons project to restricted regions of V1 (fig. S8), allowing spatially specific top-down modulation.

In addition to PV+, SOM+, and VIP+ neurons, layer 1 GABAergic neurons may also receive Cg innervation, providing both inhibition and disinhibition to pyramidal neurons (38, 39). Besides Cg projection to layer 1, other pathways may also contribute to top-down modulation, including the projection to V1 layer 6 and indirect pathways through other brain areas (16–19, 40). Furthermore, while spatial attention involves center-surround modulation in the space domain, feature attention also biases the competition between attended and unattended stimuli (1), perhaps via circuit mechanisms similar to those described here but operating in higher visual areas in stimulus feature space (41). Enhancing neuronal representation of relevant input and filtering out irrelevant stimuli are two equally important aspects of selective attention. Long-range glutamatergic projections can exert both types of modulation by activating local circuits containing distinct subtypes of GABAergic interneurons.

Supplementary Material

Refer to Web version on PubMed Central for supplementary material.

Acknowledgments

References and Notes

1. Desimone R, Duncan J. Annu Rev Neurosci. 1995; 18:193. [PubMed: 7605061]

2. Kastner S, Ungerleider LG. Annu Rev Neurosci. 2000; 23:315. [PubMed: 10845067]

3. Reynolds JH, Heeger DJ. Neuron. 2009; 61:168. [PubMed: 19186161]

4. Treue S, Maunsell JH. J Neurosci. 1999; 19:7591. [PubMed: 10460265]

5. Bisley JW, Goldberg ME. Annu Rev Neurosci. 2010; 33:1. [PubMed: 20192813]

6. Miller EK, Cohen JD. Annu Rev Neurosci. 2001; 24:167. [PubMed: 11283309]

7. Squire RF, Noudoost B, Schafer RJ, Moore T. Annu Rev Neurosci. 2013; 36:451. [PubMed: 23841841]

8. Zhou H, Desimone R. Neuron. 2011; 70:1205. [PubMed: 21689605]

9. Buschman TJ, Miller EK. Science. 2007; 315:1860. [PubMed: 17395832]

10. Gregoriou GG, Gotts SJ, Zhou H, Desimone R. Science. 2009; 324:1207. [PubMed: 19478185]

11. Moore T, Armstrong KM. Nature. 2003; 421:370. [PubMed: 12540901]

12. Noudoost B, Moore T. Nature. 2011; 474:372. [PubMed: 21572439]

13. Ekstrom LB, Roelfsema PR, Arsenault JT, Bonmassar G, Vanduffel W. Science. 2008; 321:414. [PubMed: 18635806]

14. Chen Y, et al. Nat Neurosci. 2008; 11:974. [PubMed: 18604204]

15. Sundberg KA, Mitchell JF, Reynolds JH. Neuron. 2009; 61:952. [PubMed: 19324003]

16. McAlonan K, Cavanaugh J, Wurtz RH. Nature. 2008; 456:391. [PubMed: 18849967]

17. Purushothaman G, Marion R, Li K, Casagrande VA. Nat Neurosci. 2012; 15:905. [PubMed: 22561455]

18. Sarter M, Hasselmo ME, Bruno JP, Givens B. Brain Res Brain Res Rev. 2005; 48:98. [PubMed: 15708630]

19. Saalmann YB, Pinsk MA, Wang L, Li X, Kastner S. Science. 2012; 337:753. [PubMed: 22879517]

20. Segraves MA, Goldberg ME. J Neurophysiol. 1987; 58:1387. [PubMed: 3437337]

21. The projection to superior colliculus arises only from deep layers (Fig. 1D), similar to that in primate FEF.

22. Treue S, Martinez Trujillo JC. Nature. 1999; 399:575. [PubMed: 10376597]

23. Moore T, Fallah M. J Neurophysiol. 2004; 91:152. [PubMed: 13679398]

24. Xu X, Roby KD, Callaway EM. J Comp Neurol. 2010; 518:389. [PubMed: 19950390]

25. Fishell G, Rudy B. Annu Rev Neurosci. 2011; 34:535. [PubMed: 21469958]

26. Adesnik H, Bruns W, Taniguchi H, Huang ZJ, Scanziani M. Nature. 2012; 490:226. [PubMed: 23060193]

27. Lee SH, et al. Nature. 2012; 488:379. [PubMed: 22878719]

28. Wilson NR, Runyan CA, Wang FL, Sur M. Nature. 2012; 488:343. [PubMed: 22878717]

29. Petreanu L, Mao T, Sternson SM, Svoboda K. Nature. 2009; 457:1142. [PubMed: 19151697]

30. Wickersham IR, et al. Neuron. 2007; 53:639. [PubMed: 17329205]

31. Lee S, Kruglikov I, Huang ZJ, Fishell G, Rudy B. Nat Neurosci. 2013; 16:1662. [PubMed: 24097044]

32. Madisen L, et al. Nat Neurosci. 2012; 15:793. [PubMed: 22446880]

33. Fu Y, et al. Cell. 2014; 156:1139. [PubMed: 24630718]

34. Pfeffer CK, Xue M, He M, Huang ZJ, Scanziani M. Nat Neurosci. 2013; 16:1068. [PubMed: 23817549]

35. Pi HJ, et al. Nature. 2013; 503:521. [PubMed: 24097352]

36. Mitchell JF, Sundberg KA, Reynolds JH. Neuron. 2007; 55:131. [PubMed: 17610822]

37. Based on a magnification factor of 10 μm/° in mouse V1 (Bonin et al. *J Neurosci* 31, 18506, 2011), 200 μm of cortical distance corresponds to 20° of visual angle. A previous study (26) showed that for most neurons the preferred size of visual stimulus was <15° in radius, and stimuli beyond this radius suppressed neuronal responses. This suggests that surround suppression for top-down modulation and bottom-up processing occur on similar spatial scales. The same inhibitory circuits could also contribute to decreased receptive field similarity and signal correlation between V1 neurons over ~200 μm (Bonin, et al. J Neurosci. 2011; 31:18506. [PubMed: 22171051]

38. Letzkus JJ, et al. Nature. 2011; 480:331. [PubMed: 22158104]

39. Jiang X, Wang G, Lee AJ, Stornetta RL, Zhu JJ. Nat Neurosci. 2013; 16:210. [PubMed: 23313910]

40. Mysore SP, Knudsen EI. Nat Neurosci. 2013; 16:473. [PubMed: 23475112]

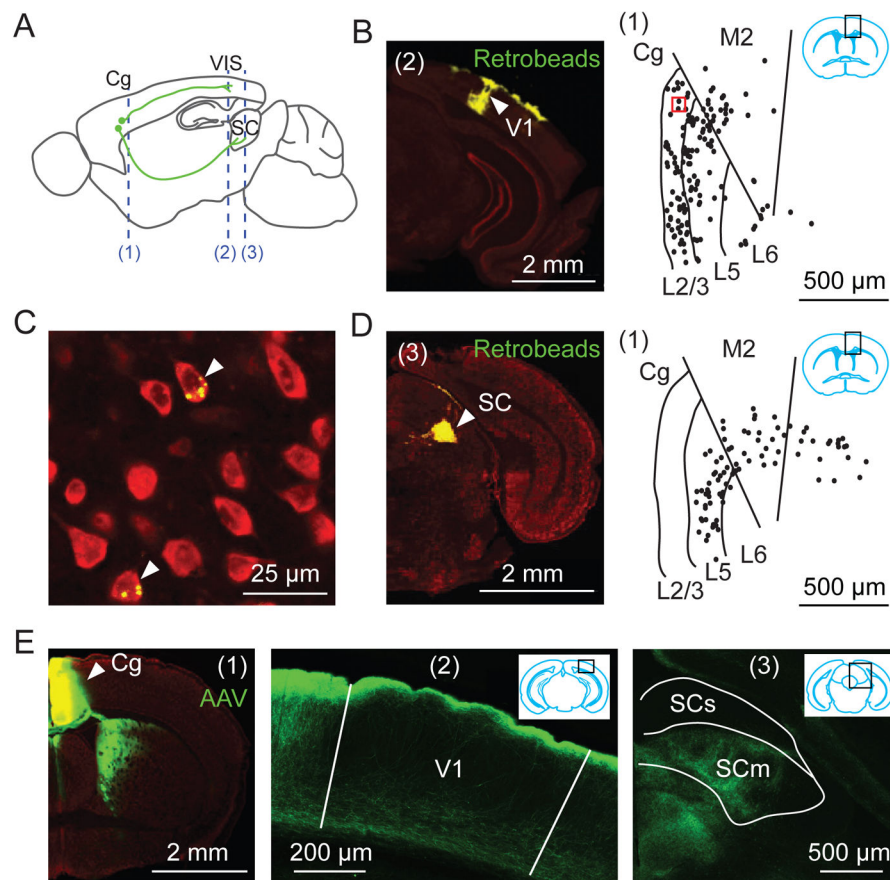41. Ardid S, Wang XJ, Compte A. J Neurosci. 2007; 27:8486. [PubMed: 17687026]

Fig. 1. Cg projects to visual cortex and superior colliculus (SC)
(A) Schematic of Cg projections. Dashed lines, locations of coronal sections shown in this figure: (1), Cg; (2), V1; (3), SC. **(B to D)** Retrograde tracing. (B) Left, Fluorescence image at location (2) showing Retrobeads (green) injected into V1. Arrowhead, injection site. Red, Nissl staining. Right, labeled neurons (dots) at (1), in region outlined by black rectangle (inset). (C) Fluorescence image for red square in (B). Arrowheads, labeled neurons. (D) Similar to (B), with Retrobeads injected into SC. **(E)** Anterograde tracing from Cg. Left, Fluorescence image at (1). Arrowhead, AAV injection site; middle and right, Cg projections to V1 and SC. SCs/SCm, sensory/motor related SC.
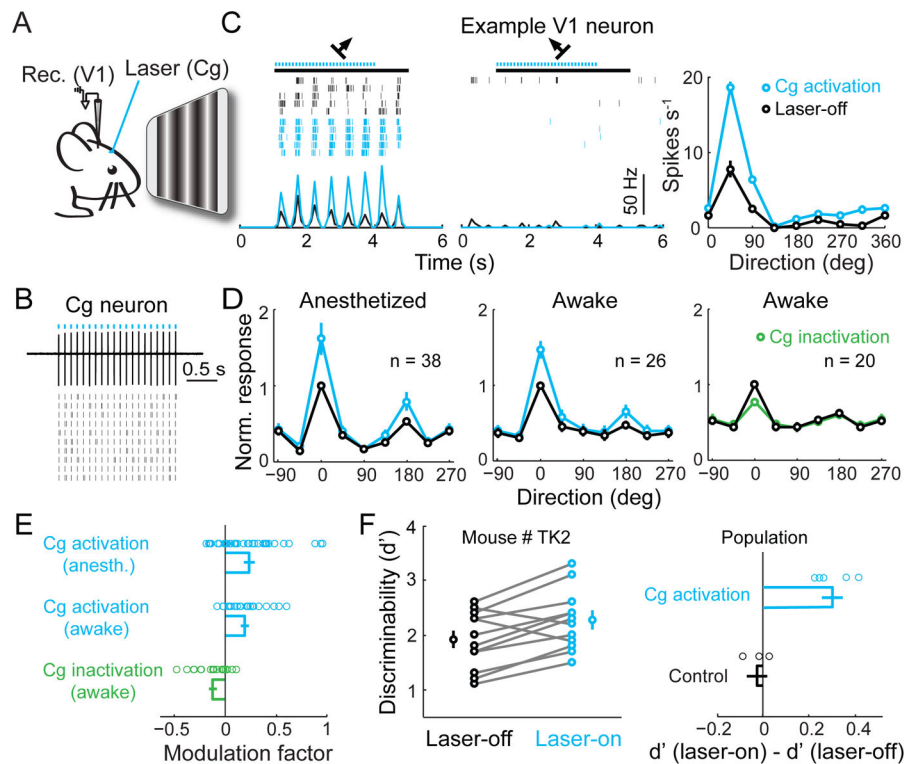
Fig. 2. Cg activation enhances V1 neuron responses and improves visual discrimination
(A) Schematic of experiment. (B) Cg neuron spiking induced by laser (5 ms/pulse, 10 Hz,
blue dots). Upper, example trace. Lower, raster plot. (C) Visual response of a V1 neuron
with (blue) or without (black) Cg activation. Left and middle, raster plots and PSTHs at
preferred and non-preferred orientations. Black bar, duration of visual stimulation (4 s).
Right, orientation tuning of this neuron. Error bar, ±SEM. (D) Population average of
orientation tuning, with each neuron normalized and aligned by its optimal orientation
without laser. Left and middle, tuning with (blue) and without (black) Cg activation in
anesthetized and awake mice. Right, tuning with (green) and without (black) Cg inactivation
in awake mice. (E) Modulation factors. Cg activation: anesthetized, 0.24 ± 0.05 (mean $\pm$
SEM), $P = 10^{-4}$ (*t*-test), $n = 38$; awake, 0.19 ± 0.04, $P = 6 \times 10^{-5}$, $n = 26$; Cg inactivation:
awake, -0.12 ± 0.03, $P = 0.003$, $n = 20$. Each circle represents one neuron. (F) Effect of Cg
activation on visual discrimination performance. Left, an example mouse. Each pair of
circles represent d′ measured in one day ($n = 11$ days). Laser-on (blue), 2.27 ± 0.16 (mean $\pm$
SEM.), laser-off (black), 1.91 ± 0.16, $P = 0.005$, paired *t*-test. Right, population summary of
laser-induced change in d′, for Cg activation (mice injected with AAV2/2-CaMKIIα-
hChR2(H134R)-EYFP, 0.30 ± 0.04, $n = 5$) and control (AAV2/2-CaMKIIα-mCherry, -0.02
± 0.04, $n = 3$) groups. $P_{laser} = 0.002$, $P_{group} = 0.59$, $P_{interaction} = 0.0009$ (two-way mixed
ANOVA); laser had significant effect only in ChR2 group ($P = 0.0006$, post-hoc Tukey's
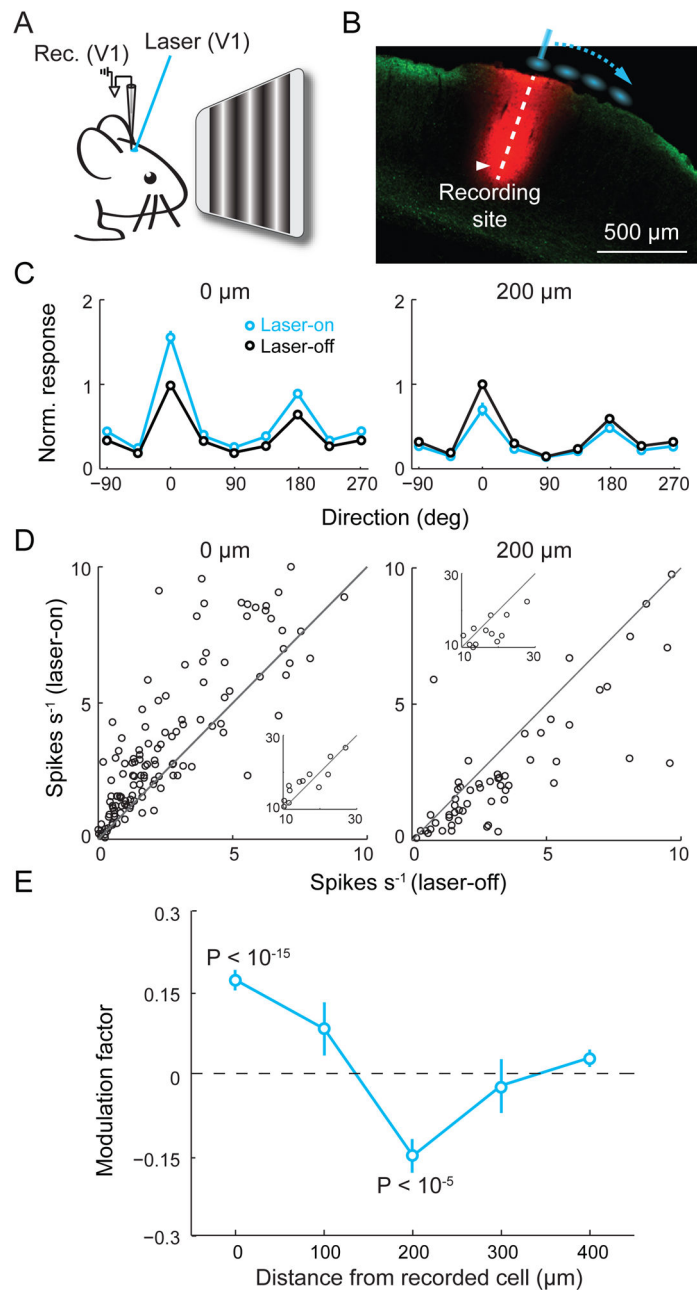test).

Fig. 3. Focal activation of Cg axons induces center-surround modulation

(A) Schematic of experiment. **(B)** Laser stimulation sites (blue) relative to recording site (red, DiI labeling). Green, Cg axons. **(C)** Average tuning curves with (blue) and without (black) laser at 0 μm ($n = 152$) and 200 μm ($n = 78$) from recorded neuron. Error bar, ±SEM. **(D)** Peak firing rate with vs. without laser for neurons with peak rates < 10 spikes s^{-1}. Inset, for peak rates > 10 spikes s^{-1}. Laser induced significant increase at 0 μm ($P = 2 \times 10^{-10}$, paired t-test) and decrease at 200 μm ($P = 3 \times 10^{-5}$). **(E)** Modulation factor vs. stimulation location. At 0 μm, 0.17 ± 0.02 (mean ± SEM), $P = 4 \times 10^{-16}$, $n = 152$; 100 μm, 0.08 ± 0.05, P

= 0.11, n = 20; 200 μm, -0.15 ± 0.03, $P = 4 \times 10^{-6}$, $n = 78$; 300 μm, -0.02 ± 0.05, $P = 0.66$, n = 18; 400 μm, 0.04 ± 0.02, $P = 0.06$, $n = 66$.
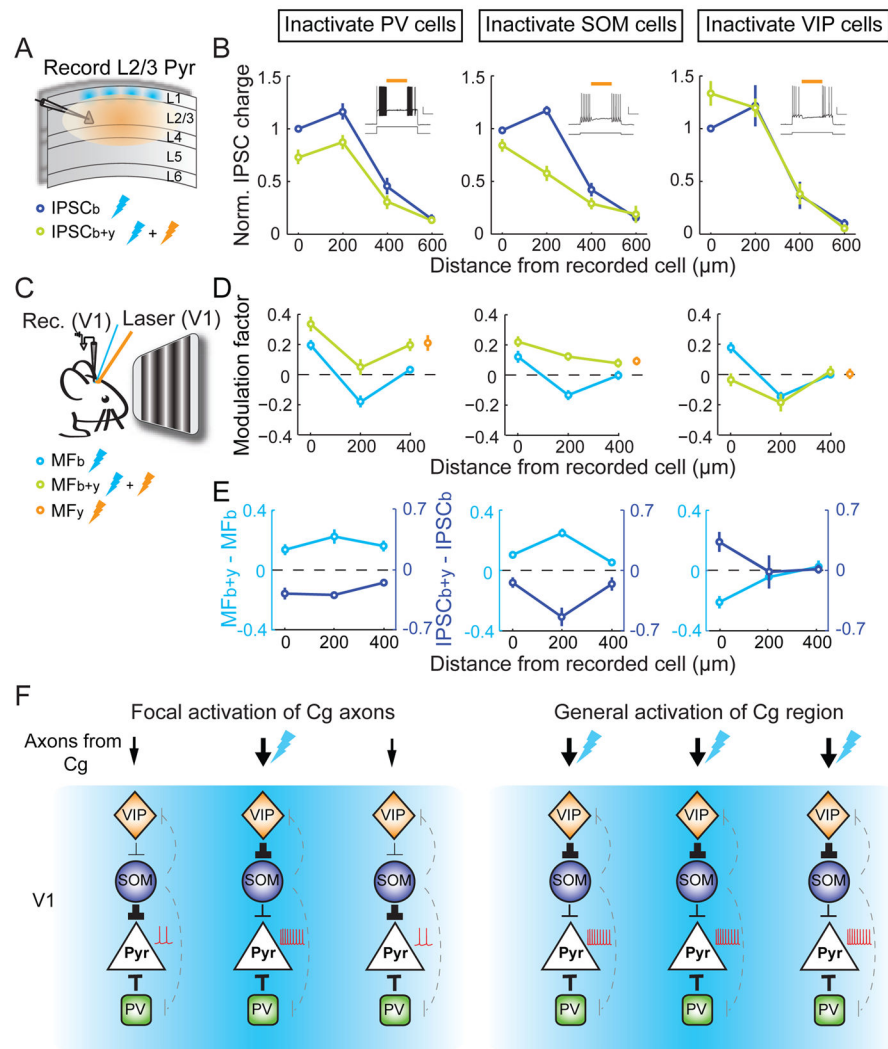
Fig. 4. Contributions of PV+, SOM+ and VIP+ neurons to disynaptic inhibition and top-down modulation

(A) Schematic of slice experiment. Thunderbolt denotes laser stimulation. **(B)** Left, normalized IPSC charge vs. blue light location with (green) or without (blue) PV+ neuron inactivation. Reduction of IPSC was found at 0 μm ($P = 0.004$, $n = 9$), 200 μm ($P = 5 \times 10^{-5}$) and 400 μm ($P = 0.009$). Inset, yellow laser suppressed firing of depolarization-induced PV+ neuron firing (top, membrane potential; yellow bar, yellow laser duration; bottom, current injection. Scale bars, 0.5 s, 20 mV/500 pA). Middle and right, inactivation of SOM+ ($n = 10$; 0 μm, $P = 0.04$; 200 μm, $P = 7 \times 10^{-4}$; 400 μm, $P = 0.04$) and VIP+ ($n = 9$; 0 μm, $P = 0.02$; 200 μm, $P = 0.92$; 400 μm, $P = 0.81$) neurons. **(C)** Schematic of *in vivo* experiment. **(D)** Modulation factor vs. location of Cg axon stimulation with (green) or without (cyan) PV+, SOM+ or VIP+ neuron inactivation (n ≥ 16 for each point). PV+ inactivation, 0 μm, $P = 0.005$; 200 μm, $P = 6 \times 10^{-4}$; 400 μm, $P = 5 \times 10^{-4}$. SOM+ inactivation, 0 μm, $P = 2 \times 10^{-4}$; 200 μm, $P = 1 \times 10^{-8}$; 400 μm, $P = 0.02$. VIP + inactivation, 0 μm, $P = 5 \times 10^{-5}$; 200 μm, $P = 0.34$; 400 μm, $P = 0.59$. Yellow circles, modulation factor with yellow light only. **(E)** Changes in modulation factor (cyan) and normalized IPSC charge (blue) induced by yellow light. **(F)**

Diagrams of V1 circuits recruited by Cg projection. Left, focal activation; right, general activation. Thunderbolt denotes site of Cg axon activation. Black lines, connections important for top-down modulation; line width represents amplitude of synaptic input. Dashed gray lines, other known connections.